J. Fluid Mech. (2010), *vol.* 648, *pp.* 5–33.
doi:10.1017/S0022112009993880

Flow regimes in a plane Couette flow with system rotation

T. TSUKAHARA†, N. TILLMARK AND P. H. ALFREDSSON

Linné Flow Centre, KTH Mechanics, Royal Institute of Technology, S-100 44, Stockholm, Sweden

(Received 3 July 2009; revised 5 December 2009; accepted 6 December 2009)

Flow states in plane Couette flow in a spanwise rotating frame of reference have been mapped experimentally in the parameter space spanned by the Reynolds number and rotation rate. Depending on the direction of rotation, the flow is either stabilized or destabilized. The experiments were made through flow visualization in a Couette flow apparatus mounted on a rotating table, where reflected flakes are mixed with the water to visualize the flow. Both short- and long-time exposures have been used: the short-time exposure gives an instantaneous picture of the turbulent flow field, whereas the long-time exposure averages the small, rapidly varying scales and gives a clearer representation of the large scales. A correlation technique involving the light intensity of the photographs made it possible to obtain, in an objective manner, both the spanwise and streamwise wavelengths of the flow structures. During these experiments 17 different flow regimes have been identified, both laminar and turbulent with and without roll cells, as well as states that can be described as transitional, i.e. states that contain both laminar and turbulent regions at the same time. Many of these flow states seem to be similar to those observed in Taylor–Couette flow.

1. Introduction

Stability and transition to turbulence in various flow systems have been studied since the pioneering works of Rayleigh (1880) and Reynolds (1883). One category of such flow systems can be classified as shear layers where inviscid and viscous instability mechanisms may give rise to instabilities. Inflection type instability, exponential growth of Orr–Sommerfeld modes and transient, algebraic growth are examples of such mechanisms and are extensively described in the monograph by Schmid & Henningson (2001). Such instabilities are important in many applications of fluid mechanics, e.g. on airfoils and in jet flows. Another type of instability may occur in flow fields which are affected by body forces. Examples of such forces are buoyancy due to density differences, centrifugal forces due to streamline curvature and Coriolis forces due to system rotation.

The 'canonical' case of buoyancy-induced instability is the so-called Bénard convection where a fluid between two infinitely large horizontal plates is heated from below. This sets up counter-rotating convection rolls and for high temperature differences various secondary instabilities may occur. The most studied flow case

† Present address: Department of Mechanical Engineering, Faculty of Science and Technology, Tokyo University of Science, Yamazaki 2641, Noda-shi, Chiba, 278-8510, Japan. Email address for correspondence: tsuka@rs.noda.tus.ac.jp

where centrifugal instability dominates is the so-called Taylor–Couette flow (hereafter TCF), where the fluid is contained between two concentric, independently rotating cylinders. The basic instability in this flow gives rise to axisymmetric vortices (often called Taylor vortices) with a cross-stream size approximately equal to the gap width. These two flows are well described in many books as for instance Chandrasekhar (1961) and Drazin & Reid (1981).

The influence of rotation on stability due to the Coriolis force is less studied. If there is a component of the rotation vector that is parallel to the wall and normal to the mean flow direction the Coriolis effects may lead to an unstable 'stratification'. As in cases where stratification is set up by density differences the flow may develop streamwise-oriented vortices. The Coriolis force may, however, be stabilizing or destabilizing depending on the direction of rotation. If the mean flow vorticity is of the opposite sign as compared to the system rotation vector, then the flow becomes unstable, whereas the flow becomes stabilized if they have the same sign. Lezius & Johnston (1976) did both linear stability calculations for a spanwise rotating laminar channel flow and investigated experimentally how a turbulent channel flow was affected. Alfredsson & Persson (1989) experimentally showed the existence of spanwise roll cells set up in a laminar channel flow and also showed secondary instabilities and transition to turbulence. It is interesting to note that instability may occur at Reynolds numbers almost two orders of magnitude smaller than predicted for the Tollmien–Schlichting waves to be unstable in the non-rotating case.

In a plane Poiseuille flow, the Coriolis force acts in such a way that in the half of the channel where the system rotation has opposite sign compared to the mean flow vorticity the flow becomes destabilized (anticyclonic rotation) whereas in the other half of the channel it becomes stabilized (cyclonic rotation). For plane Couette flow (PCF), on the other hand, because the basic flow vorticity is of the same sign across the channel, the Coriolis force will be either stabilizing or destabilizing across the full channel width.

The plane Couette flow is, maybe conceptually, the most simple shear flow; however, to build a working apparatus for flow experiments is a complex challenge. A functioning Couette flow apparatus (the principle of the apparatus is described in § 3) was constructed and built in 1990 at KTH and was used to study turbulent spots and the transition to turbulence first reported by Tillmark & Alfredsson (1990). Later, turbulent plane Couette flow was also studied and compared with results from direct numerical simulations by Bech *et al.* (1995). The basic design principle of this apparatus has later been used by several other groups, and to our knowledge at least five other apparatuses have been built based on the KTH design.

In a second phase of experiments at KTH, the PCF apparatus has been mounted on a rotating table in order to investigate the effects of system rotation. We will denote this flow rotating plane Couette flow (RPCF). Some preliminary results were given by Alfredsson & Tillmark (2005) and later Hiwatashi *et al.* (2007) studied RPCF at low Reynolds numbers to investigate some stable, three-dimensional, finite amplitude solutions which were obtained theoretically/numerically by Nagata (1998) and Nagata & Kawahara (2004). In this work, we extend the previous experimental studies and make an extensive mapping of various flow instabilities that occur in an RPCF.

As far as we know, there exist no other experimental studies on RPCF than those carried out at KTH. However, there exist a few direct numerical simulation studies of the rotating turbulent plane Couette flow. The paper by Komminaho, Lundblad &

Johansson (1996) was mainly devoted to the non-rotating case; however, they also showed that a turbulent flow can be stabilized and even relaminarize by rather weak negative rotation. Turbulent, i.e. high Reynolds number, RPCF was simulated by Bech & Andersson (1996, 1997), with destabilizing rotation, and they found that secondary flow in the form of streamwise-oriented vortices also occurs in this case both for weak and strong rotation.

1.1. *Related work*

Taylor–Couette flow is one of the most studied systems with regard to hydrodynamic stability, transition and turbulence. Although the seminal paper by Taylor (1923) was published more than 80 years ago, the richness of this flow system continues to keep researchers occupied and new phenomena are still discovered. We do not attempt to make a comprehensive review of TCF here, because there are several monographs and workshop proceedings dealing exclusively with this flow system (see e.g. Koschmieder 1993); however, we have found that many of the flow features that have been observed in TCF can also be found in the RPCF. The similarities between the two systems may partly be due to the fact that for a given experiment there are two independent control parameters in both systems: in the TCF the angular speeds of the two cylinders and in the RPCF the wall velocity and the rotational speed. In the following, we put emphasis on some research papers on TCF that are relevant for our study.

Taylor (1923) made a thorough analysis of the linear stability properties for axisymmetric disturbances of the TCF and also confirmed the results with experiments. Later, Coles (1965) made extensive and careful experiments in a relatively small gap width TCF (radius ratio $r_o/r_i \approx 1.12$) on both co- and counter-rotating cylinders and found for high rotation rates a large number of flow scenarios. He also showed that depending on how a specific point in parameter space was reached, that point could have several different flow states (i.e. different spanwise and streamwise wavenumbers of the Taylor vortices). The TCF was further studied by Andereck, Liu & Swinney (1986) in a similar geometry as that of Coles and they identified 18 principal flow regimes by careful flow visualization experiments. They also produced a map of the Re_i–Re_o plane, i.e. the parameter plane spanned by the Reynolds numbers based on the inner and outer cylinder diameters and velocities, respectively. Note that if we, by definition, let $Re_i \geqslant 0$ then Re_o can have both positive and negative values depending on if it is co-rotating ($Re_o > 0$) or counter-rotating ($Re_o < 0$).

1.2. *Motivation of present work*

There has been some recent interest in investigations of TCF when the radius ratio $r_o/r_i \to 1$. In that case, Faisst & Eckhardt (2000) showed that the TCF approaches the PCF and one could expect that the instability that leads to Taylor vortices may be overtaken by the instability that gives turbulence in the PCF. In the small gap case with co-rotating cylinders with slightly different speed, one obtains the PCF with system rotation. This is however a complicated or even impossible situation to obtain experimentally because the radius ratio needs to be around or less than 1.01 and the speeds fairly high to get into the interesting parameter regime. Carey, Schlender & Andereck (2007) recently made experiments in an apparatus with $r_o/r_i = 1.01$, but in their case only the inner cylinder was rotating. However, they found small-scale structures overlaid on the Taylor vortices which they named 'bursts'. These structures have not previously been observed for larger radius ratios.

Recently, several researchers (see e.g. Prigent *et al.* 2002; Prigent & Dauchot 2005) have observed a regular pattern of turbulent stripes interweaved with laminar regions

that are inclined to the flow direction, in both PCF and TCF. This kind of transition scenario has been observed in different flow systems and described by a process called 'spatiotemporal intermittency'. Especially, a state well known as 'spiral turbulence' was discovered in a counter-rotating TCF by Coles (1965) and was further studied experimentally (Andereck *et al.* 1986; Hegseth *et al.* 1989). Similar patterns have been numerically reproduced in PCF by Barkley & Tuckerman (2005, 2007) and also in a plane Poiseuille flow by Tsukahara *et al.* (2005). However, its self-organizing mechanism is still a question attracting much attention from researchers.

In this work, we are studying the RPCF in a plane channel with system rotation. We have previously made some preliminary studies that have shown that this flow system contains a number of different flow states, many of them seem similar to those observed in the TCF. However, the RPCF have some advantages over the TCF: one is that geometry is simple and one can directly distinguish how the Coriolis force enters the flow equations. We propose that RPCF is probably a better model system to work with in order to investigate nonlinear flow instabilities and bifurcations than the TCF system, from both theoretical and numerical perspectives. From an experimental point of view, it is of course a more complex apparatus than usually needed for TCF experiments; however, to obtain true RPCF at high Re it is the only possibility.

The layout of the paper is as follows. Section 2 gives a brief introduction to the equations of motion and the relevant parameters and also compares with other similar systems, especially the TCF system. The experiments are described in § 3, with respect to both the set-up and the experimental procedure. In the experiments, a number of different flow states have been observed, and in § 4 we classify the different states and map them in the Re–Ω plane, where Ω is a non-dimensional rotation number as defined in the following section. Section 5 describes, mainly through photographic evidence, these states and gives some quantitative results about scales obtained from evaluating the patterns in the photographs. Finally, § 6 gives the conclusions of the present work and also gives some indications for future work.

2. Theoretical background

2.1. *Governing equations*

The momentum and continuity equations for a flow in a rotating frame of reference with an angular velocity $\boldsymbol{\Omega} = \boldsymbol{\Omega}(t)$ are

$$\frac{\partial \boldsymbol{u}}{\partial t} + \boldsymbol{u} \cdot \nabla \boldsymbol{u} = -\frac{1}{\rho}\nabla P + \nu \nabla^2 \boldsymbol{u} + 2\boldsymbol{u} \times \boldsymbol{\Omega} + \dot{\boldsymbol{\Omega}} \times \boldsymbol{r}, \tag{2.1}$$

$$\nabla \cdot \boldsymbol{u} = 0, \tag{2.2}$$

where ρ is the fluid density and ν is the kinematic viscosity, which both here are assumed to be constant. The static pressure P^* and the centrifugal acceleration are combined to give

$$P = P^* - \frac{\rho}{2}|\boldsymbol{\Omega} \times \boldsymbol{r}|^2$$

and $\boldsymbol{r}$ is a position vector from the axis of rotation. In the following, we assume that the walls are counter-moving with a velocity difference of $2U_w$ and that the distance between the walls is $2h$. For undisturbed laminar flow, the velocity profile also becomes linear in the case with system rotation so that

$$U(y) = U_w \frac{y}{h}, \tag{2.3}$$

where we chose the coordinate system such that x is in the streamwise direction, y is normal to the walls and z is in the spanwise direction. The rotation vector is in the spanwise direction, i.e. $\boldsymbol{\Omega} = \Omega_z \boldsymbol{e}_z$.

This flow can be fully characterized through two non-dimensional parameters: the Reynolds number $Re = U_w h/\nu$ and a rotation number $\Omega = 2\Omega_z h^2/\nu$. In some earlier studies, a rotation number defined as $Ro = 2\Omega_z h/U_w = \Omega/Re$ has been used; however, for this work we chose Ω to characterize the effect of rotation. In this way, Re and Ω can be changed independently in the experiment by changing the wall velocity and the system rotation speed, respectively.

The flow develops along various time scales and at least three relevant scales can be identified:

$$\tau_d = h^2 \nu^{-1} \quad - \text{diffusion time scale}, \tag{2.4}$$

$$\tau_o = h U_w^{-1} \quad - \text{outer time scale}, \tag{2.5}$$

$$\tau_\Omega = 2\pi \Omega_z^{-1} \quad - \text{rotation time scale}. \tag{2.6}$$

These time scales are related as

$$\tau_d = Re\ \tau_o = \frac{1}{4\pi} Re\ Ro\ \tau_\Omega. \tag{2.7}$$

2.2. *Linear stability of plane rotating Couette flow*

It is well known that linear stability theory predicts a stability boundary for streamwise-oriented roll cells for RPCF as

$$Re = \Omega + \frac{107}{\Omega}, \tag{2.8}$$

which gives a minimum Reynolds number for instability of 20.7 at $\Omega = 10.3$ (see e.g. Lezius & Johnston 1976; Hiwatashi *et al.* 2007). It is also well known that linear theory utterly fails when predicting instability in PCF, since according to linear theory there is no instability even for infinite Reynolds numbers, whereas experiments have already shown that turbulent spots can become self-sustained even at Reynolds numbers as low as $Re = 360$ (Tillmark & Alfredsson 1990; Daviaud, Hegseth & Bergé 1992; Prigent *et al.* 2002).

2.3. *Rotation effects on turbulence*

System rotation also affects turbulent flows through the influence of the Coriolis term. The equations for the Reynolds stresses are obtained by taking the ith component of (2.1) and multiplying by u_j and thereafter taking the ensemble average to get

$$\left(\frac{\partial}{\partial t} + U_k \frac{\partial}{\partial x_k}\right) R_{ij} = P_{ij} + \Pi_{ij} - \varepsilon_{ij} + D_{ij} + G_{ij}, \tag{2.9}$$

where $\boldsymbol{u} \cdot \boldsymbol{e}_k = U_k + u_k$, and U_k and u_k are the ensemble average and fluctuating part of the kth component, respectively. Here, $R_{ij} = \overline{u_i u_j}$, where the overbar denotes ensemble average. The first four terms on the right-hand side represent turbulent production (P_{ij}), pressure strain redistribution (Π_{ij}), viscous dissipation (ε_{ij}), turbulent and viscous diffusion (D_{ij}) and are the same as for the non-rotating case. The last term G_{ij} is a term stemming from the system rotation, which can be written as

$$G_{ij} = -2\Omega_k (R_{jm}\epsilon_{ikm} + R_{im}\epsilon_{jkm}), \tag{2.10}$$

where ϵ_{ijk} is the permutation tensor. As is well known, the Coriolis term does not perform work, so the physical interpretation of this term is a redistribution of energy

between the velocity components. It is noteworthy that the term $\dot{\boldsymbol{\Omega}} \times \boldsymbol{r}$ in (2.1) does not contribute to (2.9).

For unidirectional flows (as e.g. channel flows) there is no variation of mean quantities in the $x_1 = x$ and $x_3 = z$ directions and the mean velocity components $U_2 = U_3 = 0$. This simplifies (2.9) significantly (see e.g. Johnston, Halleen & Lezius 1972) and we can write

$$\frac{\partial}{\partial t}(\overline{u^2}) = -2\overline{uv}\left(\frac{\mathrm{d}U}{\mathrm{d}y} - 2\Omega\right) + \Pi_{11} - \varepsilon_{11} + D_{11}, \tag{2.11}$$

$$\frac{\partial}{\partial t}(\overline{v^2}) = -4\overline{uv}\Omega + \Pi_{22} - \varepsilon_{22} + D_{22}, \tag{2.12}$$

$$\frac{\partial}{\partial t}(\overline{w^2}) = \Pi_{33} - \varepsilon_{33} + D_{33}, \tag{2.13}$$

$$\frac{\partial}{\partial t}(-\overline{uv}) = \overline{v^2}\frac{dU}{dy} + 2(\overline{u^2} - \overline{v^2})\Omega + \Pi_{12} - \varepsilon_{12} + D_{12}. \tag{2.14}$$

For a steady flow, i.e. U and Ω are both independent of t, (2.11)–(2.14) can be further simplified because then the left-hand side is equal to zero.

In the case when Ω and $\partial U/\partial y$ have the same sign, turbulent energy will be transferred from the streamwise to the wall normal component. It is not obvious what the overall result will be on the turbulence, except that it will lead towards an equalization of the two components. On the other hand, negative rotation will give a transfer of energy to $\overline{u^2}$ and a decrease in $\overline{v^2}$. The normal velocity is important for turbulence production because it directly influences $\overline{uv}$ (see (2.14)) and it can be intuitively understood that negative rotation will lead to a decrease in $\overline{uv}$ and hence in a decrease in the production of turbulent energy.

2.4. *Relation to other flows*

The linear stability of the rotating Couette flow has its analogue in two other well-known flows, namely Bénard convection and Taylor–Couette flow in the small gap limit. In fact, the governing equations and boundary conditions for obtaining the stability boundary are the same except that the stability parameters are different in the three cases. In the case of Bénard convection, there is only one parameter, namely the Rayleigh number which for a given set-up can be varied by changing the temperature gradient between the plates. For TCF with only the inner cylinder rotating, the equation can be written with only one parameter, namely the Taylor number; however, in an experiment, two independent parameters can influence the flow, i.e. the individual angular speed of the two cylinders. Also, in the present case, we have two independent parameters: Re and Ω. It may therefore not be surprising that the RPCF and the TCF have many similarities when comparing various flow structures above the critical parameter values that denote instability. In both cases the origin of the instability is a body force, in the TCF it is of centrifugal origin and therefore proportional u^2 and in the RPCF it is caused by the Coriolis force and hence in linear proportion to u.

3. Experimental description

3.1. *Experimental flow apparatus*

The experiments have been carried out in a water channel mounted on a rotating table previously described by Alfredsson & Tillmark (2005) and Hiwatashi *et al.*

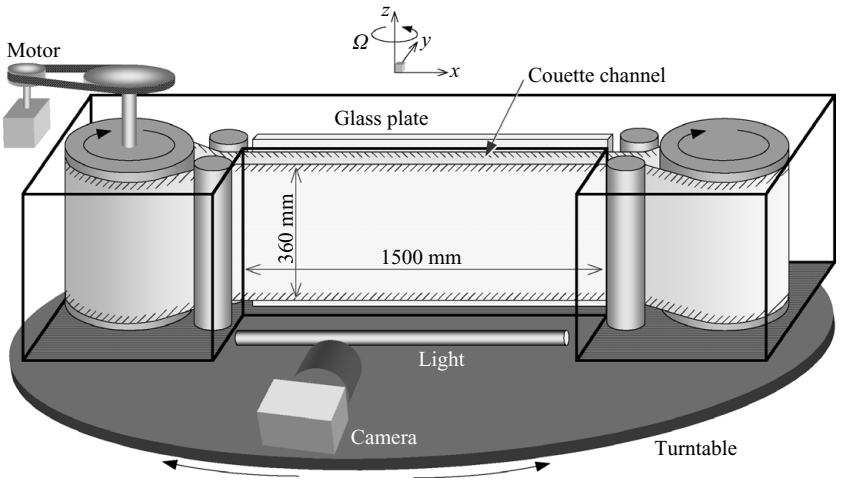

FIGURE 1. Schematic of the rotating plane Couette flow apparatus.

(2007). A schematic of the set-up is depicted in figure 1. The Couette apparatus with counter-moving walls is basically the same as in the experiment by Tillmark & Alfredsson (1990, 1992). Such a system of two counter-moving walls gives a zero net transport of fluid through the channel and, hence, non-intrusive measurement, e.g. visualization, is desired to prevent disturbance generation.

The Couette channel itself consists of two open tanks connected by a long open plane channel formed with two vertical parallel glass plates. The gap between the two sides of the channel can be changed by adjusting one of these glass plates, which is positioned inside the tank. In the present experiments, the rectangular cross-section of the channel is $10 \times 400\,\mathrm{mm}^2$, and the test section length is about 1.5 m. To form the plane Couette flow, two vertical cylinders in each tank drive an endless transparent polyester plastic belt of 360 mm width and 0.1 mm thickness. The belt, which is made of a 5 m long film with the edges glued together in a thin joint, runs along the facing inner glass surfaces of the channel. A thin lubricating water film is established and reduces friction between the band film and the glass walls. The actual distance between the plastic film surfaces, which determines the channel height ($2h$), has been measured with a microscope. The measurements need to be carried out when the belt is moving. First, the microscope, which has a very small depth of view, is focused on the inner surface, and then it is moved and focused on the outer surface. The displacement of the microscope is measured with a micrometre, and by taking the refractive index of water into account, the distance between the bands can be determined. The repeatability of the measurements has been found to be within ± 0.2 mm for a trained experimentalist.

The variation in the long-time stability of the belt speed was less than 2 %. In the remainder of this paper, x is in the streamwise direction, y is in the wall-normal direction and z is in the spanwise direction as shown in figure 1.

A turntable, on which the heavy apparatus as mentioned above is placed, is driven by a DC motor and rotates around the vertical z axis. The maximum angular velocity for the system is $\Omega_z = 0.58$ rad s^{-1} and this corresponds to a non-dimensional maximum rotation rate of $\Omega = \pm 30$. The angular velocity has been found to be constant within ± 1 %.

3.2. *Flow visualization and image processing*

This study is based on observations made through flow visualization. Visualization of the flow states has been accomplished by seeding the water used as the working fluid, with light-reflecting flakes and illuminating its whole width at an oblique angle from below (with a fluorescent light tube). Titanium-dioxide-coated mica platelets (Merck, Iriodin 120, 5–25 μm in diameter) have been chosen for the flow visualization.

Interpretation of photographs of flow visualized with these flakes is based on the fact that a disk-shaped particle aligns itself along the direction of principal axes of the local rate-of-strain tensor: for a detailed discussion, see Savaş (1985) and Barth & Burns (2007). Thus, the reflected light from the particles clearly revealed areas of turbulent and perturbed laminar flow, while the reflective light in a simple laminar flow is steady and homogeneous. This method of flow visualization has previously been used to visualize vortex structures and turbulent spots (e.g. Andereck *et al.* 1986; Tillmark & Alfredsson 1992; Prigent *et al.* 2002).

Photographs of the visualized flow pattern have been taken by a digital camera (Nikon D50) mounted on the rotating table and subsequently digitized and analysed by image processing. The camera has a maximum resolution of 3008×2000 pixels; however, all photographs have been taken with a smaller resolution of 1504×1000 pixels. Most photographs have been taken with a short exposure time giving a snapshot of the instantaneous flow field. However, in some cases a longer exposure time has been used which averages out small-scale structures and therefore clearly shows persistent large scale structures in the flow.

Several methods of illuminating the flow have been tried, and the best contrast was found by having the light source placed on the lower side of the channel. This gives rise to an inhomogeneous light intensity in the spanwise direction (vertical axis in the photographs), but we have applied digital image processing in order to separate such inhomogeneous background light intensity from the photographs. In the flow-visualization figures in this paper, the background, which can be obtained by averaging a number of realizations (at least 30 photographs which are separated in time so that even if there is a steady pattern it has moved sufficiently not to give a structure in the averaged picture), has been subtracted from each photograph.

The photographs in this paper all show a region with 1504×565 pixels. The centre-to-centre pixel spacing corresponding to the effective size in the fluid is about 0.5 mm, i.e. $h/10$. After digitalization and the above-mentioned background subtraction, the light intensity of each pixel, $I(\boldsymbol{x}) = I(x, z)$, is normalized with the maximum and minimum values in the relevant photograph:

$$I'(\boldsymbol{x}) = \frac{I(\boldsymbol{x}) - I_{min}}{I_{max} - I_{min}}. \tag{3.1}$$

Thus, $I'(\boldsymbol{x})$ ranges from 0 to 1.

To perform the statistical analysis of the scales of structures in the RPCF, we have computed the correlation function for the processed photographs. A correlation of the light intensity between spatially separated points of $\boldsymbol{x}$ and $\boldsymbol{x} + \Delta\boldsymbol{x}$ is defined as

$$R(\Delta\boldsymbol{x}) = \frac{\overline{I''(\boldsymbol{x})I''(x + \Delta\boldsymbol{x})}}{\sqrt{\overline{(I''(\boldsymbol{x}))^2}}\sqrt{\overline{(I''(\boldsymbol{x} + \Delta\boldsymbol{x}))^2}}}, \tag{3.2}$$

where $I''(\boldsymbol{x})$ is the deviation from the averaged value as given by

$$I''(\boldsymbol{x}) = I'(\boldsymbol{x}) - \overline{I'(\boldsymbol{x})}. \tag{3.3}$$

3.3. *Experimental procedures*

The experiments on a *circular* Couette flow by Coles (1965) demonstrated significant hysteresis, in which several flow states (defined by the number of cells along the axis of rotation and the number of azimuthal waves) could be obtained at the same point in parameter space. This non-uniqueness is caused by the nonlinearity of the system and the state obtained for a certain parameter combination may depend on the path followed in parameter space. Therefore, a well-prescribed path in parameter space has been specified in this study, where two different procedures were followed. In one denoted Case-Re, the Reynolds number is fixed while the rotation number is increased; whereas in Case-Ω the rotation number is fixed while the Reynolds number is decreased.

The protocol of Case-Re is that, first the film belt of the Couette apparatus is slowly accelerated from rest to its final Reynolds number with the turntable at rest, and then the turntable is slowly accelerated from rest to an aimed rotation rate ($Re = \text{const.}$, $\Omega = 0 \rightarrow \pm 30$). During the start up, the rotation rate usually reached steady state before changes in the laminar or turbulent flow were observed.

In Case-Ω, an initial flow state is established to be fully turbulent at approximately $Re = 1000$ before accelerating the rotation to a constant rotation rate. Then the belt speed is slowly decreased to an aimed Reynolds number with the constant rotation number ($Re = 1000 \rightarrow 0$, $\Omega = \text{const.}$).

It is necessary to wait a long time before observation of a state of equilibrium. In our experiments, τ_Ω (see § 2.1) is often one of the longest time scale: for instance, $\tau_\Omega \approx 280$ s for $\Omega = 1$. All pictures presented in this paper have been taken after at least 5 min after setting the control parameters. As in cases where underlying structures are seen to be unstable or intermittent, we watched further and ensured that it showed the intrinsic feature for the relevant condition.

4. Classification of flow states and structures

The principal result of this study is the complex transition diagram shown in figure 2. The abscissa of the diagram gives the rotation speed, negative values are cyclonic (i.e. stabilizing) whereas positive values are anti-cyclonic (i.e. destabilizing), and the ordinate is the Reynolds number. As can be seen, there are a number of demarcation lines in the diagram that distinguishes various flow structures identified in the experiments. More than 400 different observations have been made to obtain this diagram following the two different protocols described in § 3.3.

The structure of the flow can be classified in different ways; we chose to describe the flow by two different categories. The first category describes the flow field in general, i.e. laminar or turbulent—with 'turbulent', we mean any type of flow state that shows structures with a range of length scales, which appear disordered or chaotic. Such flows can range from being transitional to fully turbulent—unsteady or steady, and we find it relevant to define seven different *flow states* which are given in table 1. The second category defines the dominating roll-cell structure of the flow field and six different *flow structures* (including no roll cells) are found to be appropriate; see table 2. After we have done this classification, it is possible to construct a map of various flow regimes, which is given in table 3. As can be seen, 17 different flow regimes have been classified during the search of the parameter space of the present experiments.

Figures 2–5 show where, in the parameter space spanned by Re and Ω, the various flow states exist. Figure 2 gives an overview for both positive and negative Ω

COU	=	Laminar Couette flow
QTR	=	Quasi turbulence
CNT	=	Contained turbulence in roll cell
INT	=	Intermittent turbulence
SPT	=	Turbulent spots
TRS	=	Turbulent stripe
TUR	=	Turbulent flow

TABLE 1. Classification based on flow state.

N	=	No roll cells
2D	=	Two-dimensional roll cell
2Dh	=	Two-dimensional roll cell for high Ω
2Dm	=	Two-dimensional meandering roll cell
3D	=	Three-dimensional roll cell
3Ds	=	Three-dimensional spatio-temporally roll cell

TABLE 2. Classification based on flow structures.

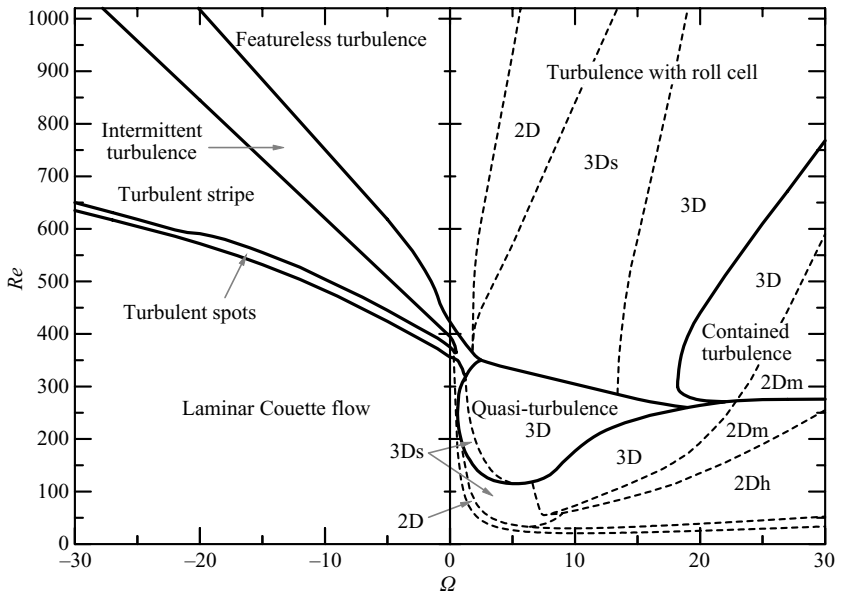

FIGURE 2. Flow regimes diagram as a function of Reynolds number Re and rotation number Ω in a plane Couette flow subject to system rotation. Solid lines indicate the transition boundaries that separate flow states, such as 'laminar flow', 'turbulent flow', 'quasi turbulence', 'intermittent turbulence' and 'contained turbulence in roll cells'. Dashed lines indicate demarcation between 'two-dimensional' and 'three-dimensional roll cells': 2Dm, meandering two-dimensional roll cell; 2Dh, straight two-dimensional roll cell observed for high rotation rates; 3Ds, spatio-temporally intermittent three-dimensional roll cell. More details are shown in figure 3 for low Reynolds number, and shown in figures 4 and 5 for positive-rotating and negative-rotating systems for high Reynolds numbers, respectively.

spanning the range ± 30 and for Re up to 1000. The solid lines show the demarcation between the different flow states given in table 1, whereas the dashed lines show the demarcation between different flow structures (see table 2) within a given flow state. As can be seen, it is a fairly complicated diagram, and the demarcations between different regions are in some cases not clear-cut.

	N	2D	3D	3Ds	2Dm	2Dh
COU	COU	COU2D	COU3D	COU3Ds	COU2Dm	COU2Dh
QTR	–	–	QTR3D	QTR3Ds	–	–
TUR	TUR	TUR2D	TUR3D	TUR3Ds	–	–
CNT	–	–	CNT3D	–	CNT2Dm	–
INT	INT	–	–	–	–	–
SPT	SPT	–	–	–	–	–
TRS	TRS	–	–	–	–	–

TABLE 3. The principal regimes observed in a plane Couette flow with system rotation.

Figure 3 shows an enlargement of the region $0 \leqslant Re \leqslant 400$ and $0 \leqslant \Omega \leqslant 30$, where a large number of both flow states and flow structures can be found. In this figure as well as in figures 4 and 5, each symbol represents an experimental observation, and the heading of the figure shows which procedure has been used (i.e. Case-Ω or Case-Re). In all cases, we have found that the flow state observed at a given point in the Re–Ω plane does not depend on how that point is approached. In figure 4, the region $200 \leqslant Re \leqslant 1050$ and $0 \leqslant \Omega \leqslant 30$ is instead shown, whereas figure 5 shows a similar diagram for stabilizing rotation. In § 5, we will describe the flow structures in the various regions in detail based on flow visualization.

5. Flow regimes determined from experiments

In the following, we will take the reader through the varying landscape of RPCF and describe the various regimes. We will use table 3 to keep track of the different regimes and will follow it row by row. Each section in the following corresponds to one or a group of neighbouring flow states, and the corresponding flow structures are described in some detail. In all cases, one or several photographs are used to illustrate the flow state. We will also point out common features with flow regimes observed in TCF where appropriate.

5.1. *Laminar Couette flow (COU)*

5.1.1. *Laminar Couette flow: no roll cells*

The laminar Couette flow regime with no imbedded roll cells or other structures occupies a fairly large part of figure 2. For no rotation the results obtained in this study confirm the results from Tillmark & Alfredsson (1992) that below $Re = 360$, the flow is laminar and all turbulent disturbances will decay, while other observations in slightly different experimental configurations and numerical simulations have revealed lower or higher values of the critical Reynolds number in the range of 320–370 (Lundbladh & Johansson 1991; Daviaud *et al.* 1992; Dauchot & Daviaud 1995). This is obtained using the protocol Case-Ω where the Reynolds number is sequentially decreased, Ω being maintained at zero. For stabilizing rotation $\Omega < 0$, the laminar region is extended to higher Reynolds numbers. For instance, for $\Omega = -25$ laminar flow is obtained up to $Re \approx 600$. The good agreement with Tillmark & Alfredsson (1996) is even more satisfactory when one takes into account the fact that their channel width was 20 mm, whereas in this study it is 10 mm.

For positive Ω, the simple PCF is found to exist below the curve given by (2.8) in accordance with the results of linear stability theory and the previous results of Tillmark & Alfredsson (1996).

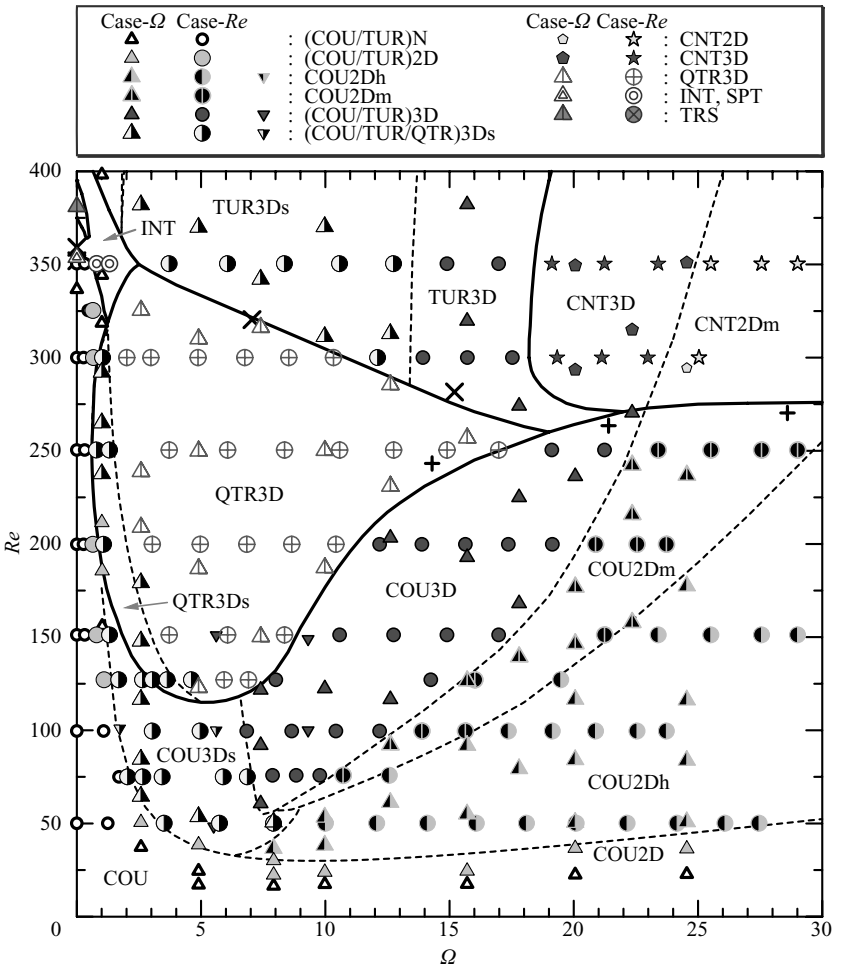

FIGURE 3. Flow regimes diagram for low Reynolds numbers in the case of positive rotating. A triangle, cf. △, indicates Case-Ω, a circle indicates Case-Re, and an inverted triangle indicates the experimental result obtained by Hiwatashi *et al.* (2007). Color of the symbol displays an individual flow state and structure. The symbols (×) and (+) indicate demarcation between laminar and turbulent flows by previous experiments (Tillmark & Alfredsson 1996; Alfredsson & Tillmark 2005).

When entering the laminar region from a fully turbulent one, for instance by starting at a high Reynolds number and then decreasing it, the situation in figure 6 usually occurs. In the figure, a rotation number of $\Omega = -14.9$ is shown to dramatically affect the flow, which should be fully turbulent under a non-rotating condition, and in figure 6(*b*) no turbulent motions are visible. The turbulence dies away and usually a turbulent region forming a turbulent spot remains and may move slowly around until it finally decays and the flow becomes fully laminar. The turbulent spot is clearly observed in the photograph and even more clearly by direct observation with the naked eye. If one is close to the stability border, the relaminarization process may take a significant time (i.e. between several and up to 30 min).

5.1.2. *Two-dimensional roll cell in laminar flow*

According to linear stability theory, two-dimensional roll cells will form above the boundary given by (2.8). A typical photograph of such structures is shown in figure 7.

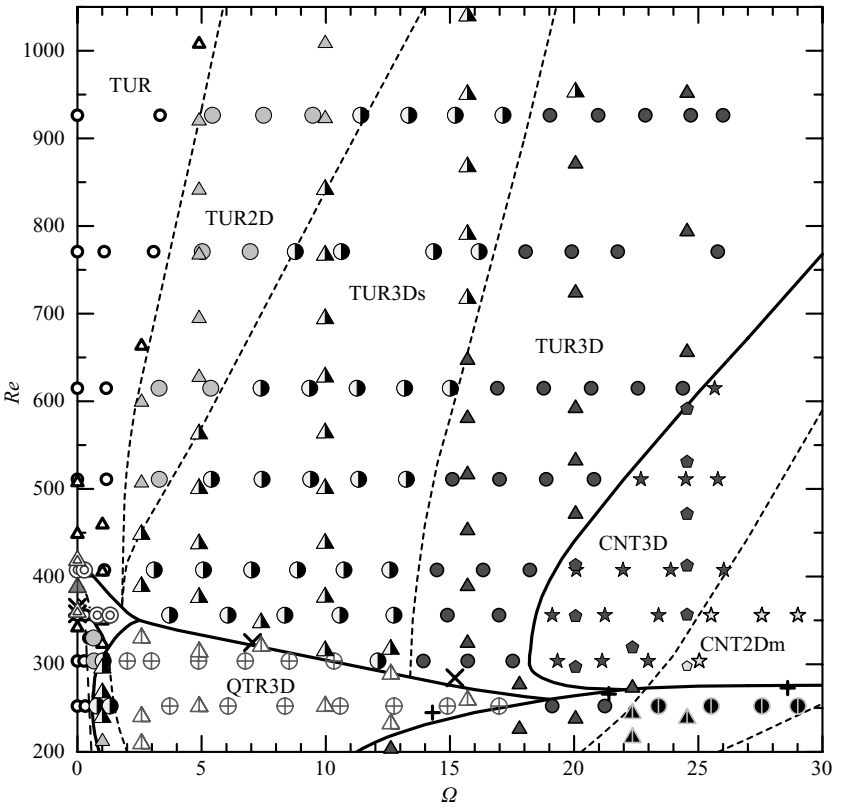

FIGURE 4. Same as figure 3 but for high Reynolds numbers in the case of positive rotating.

Here $Re = 50.6$ and $\Omega = 2.58$. At this Ω, the critical Re is 44, so we are only slightly above the stability line.

The structures are, as can be seen, quite two-dimensional and steady, although a slight drift of the structures towards the free surface was observed. The wavelength is larger in the lower part of the channel and probably due to Ekman layers forming at the solid boundary there.

When visualizing structures with reflective flakes, the resulting image depends on both the location of the light source with respect to the flow structures and the location of the observer. A tentative example of the visualization of non-symmetric spanwise-oriented roll cells is seen in figure 7(*b*), where we have assumed that the platelets on average orient themselves with the streamlines.

To obtain the average spanwise wavelength of the pattern, we use a correlation technique that correlates the brightness in the photograph. We make this correlation only in the upper part of the channel to avoid the influence from the lower wall. As can be seen from figure 8, this technique gives a strong spanwise correlation from which the spanwise wavelength can be estimated to be $4.0h$. This compares well with the spanwise scale of a roll-cell pair calculated from linear stability theory and with the picture in figure 7(*b*).

5.1.3. *Three-dimensional roll cell in laminar flow*

We have also observed steady three-dimensional disturbances in a rather small region of the Re–Ω parameter space. Two such cases are displayed in figure 9. The photographs show a quite surprisingly regular pattern over the full view, although

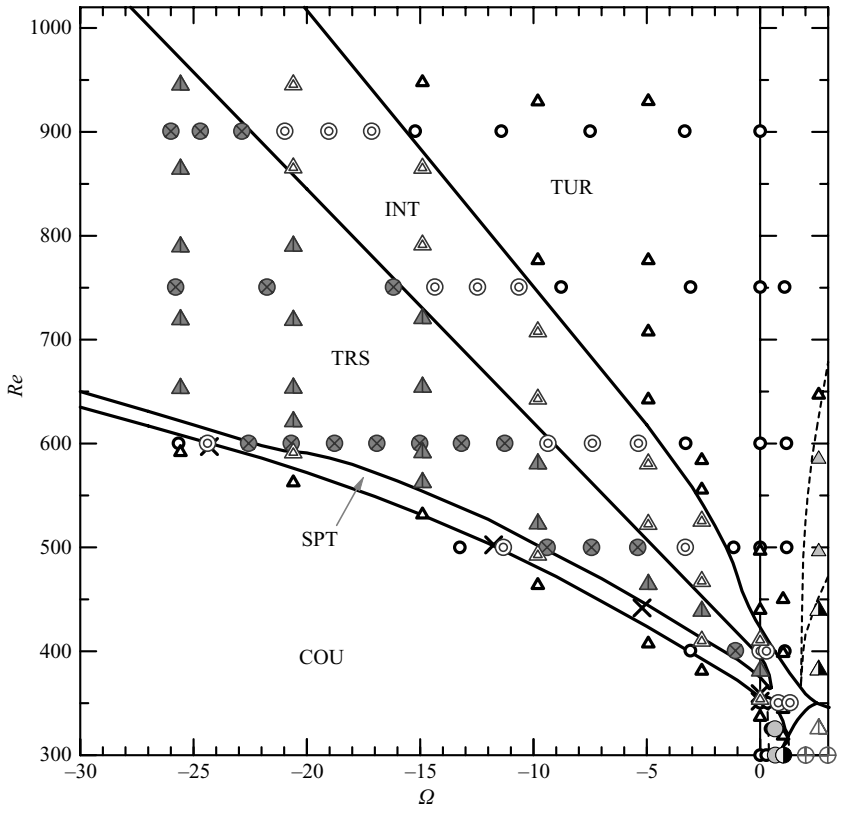

FIGURE 5. Same as figure 3 but for high Reynolds numbers in the case of negative rotating.

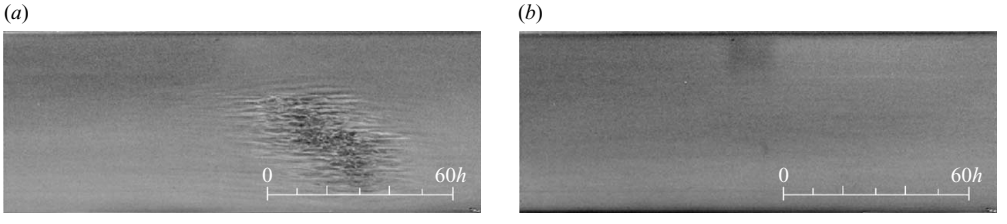

FIGURE 6. Front view photograph of the flow: laminar flow (COU) at $Re = 531$, $\Omega = -14.9$. A turbulent spot in (a) decays, and the flow becomes laminar 200 s after, as shown in (b).

there is also a slightly larger wavelength close to the bottom of the channel. The case shown in figure 9(a) is close in parameter space to one stable case reported by Hiwatashi *et al.* (2007), which was also predicted theoretically by Nagata (1998).

5.1.4. *Unstable three-dimensional roll cells (COU3Ds) and quasi-turbulence (QTR)*

In between the regions of two-dimensional and three-dimensional roll cells, there exist regions that are spatially and temporally intermittent, meaning that two- and three-dimensional roll cells develop, interact, break down and disappear intermittently.

In figure 10, we show a sequence of four photographs showing how the flow field, which basically consists of two-dimensional roll cells, at some random regions suddenly develop a number of three-dimensional cells that exist for some time before disappearing. In figure 10, two such regions develop: in figure 10(b) one

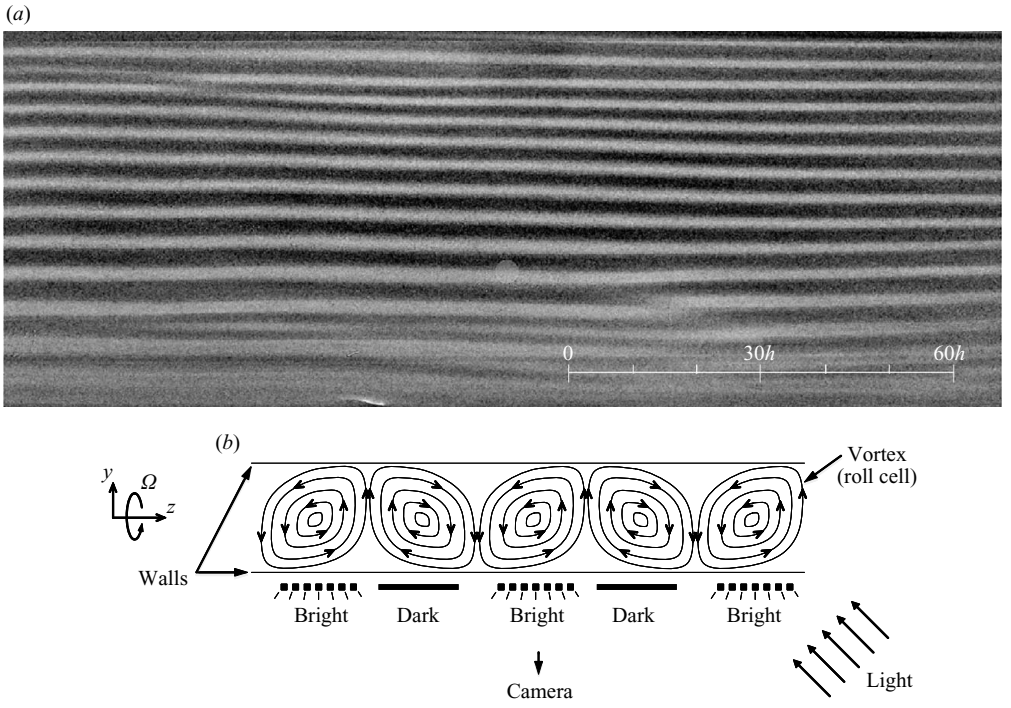

FIGURE 7. (*a*) Stable two-dimensional roll cells in laminar flow (COU2D); $Re = 50.6$, $\Omega = 2.58$. (*b*) Relation between roll cells and brightness reflected by flakes.

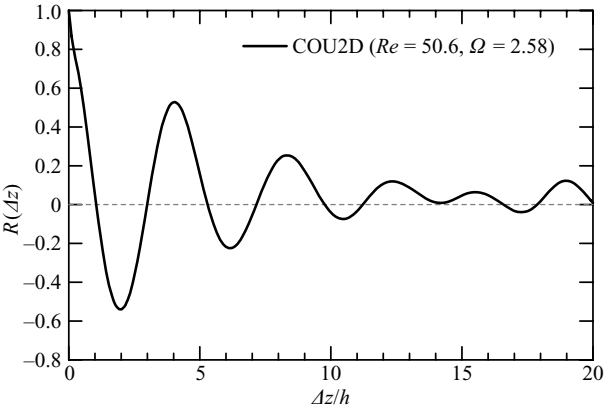

FIGURE 8. Two-point correlation coefficient of light intensity, for the laminar flow with stable two-dimensional roll cells (corresponding to the cases shown in figure 7), as a function of the spanwise distance Δz.

is fairly well developed on the left-hand side of the photograph, whereas one is starting in the right-hand side. Figure 10(*c*) shows how the one on the left-hand side dies away, whereas the other has grown in amplitude. Finally, in figure 10(*d*) the flow again consists of two-dimensional roll cells. The wavy structure of the three-dimensional cells is not stable but decays in amplitude and a pattern of nearly straight cells is again formed. In other words, two-dimensional roll cells intermittently and locally change into three-dimensional roll cells without turbulent-like motion as

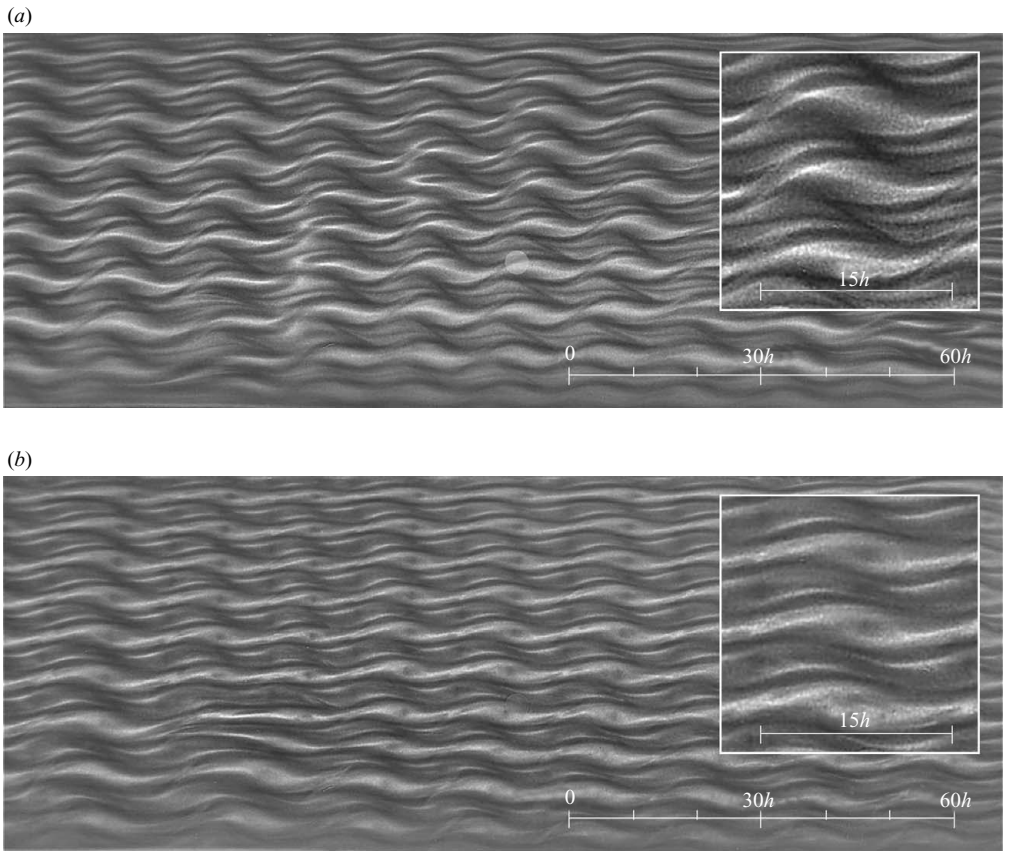

FIGURE 9. Stable three-dimensional roll cells in laminar flow (COU3D); (*a*) $Re = 99.6$, $\Omega = 8.65$; (*b*) $Re = 200$, $\Omega = 17.4$. The rectangle show a blow-up of the centre part of the pictures with a factor of 2.

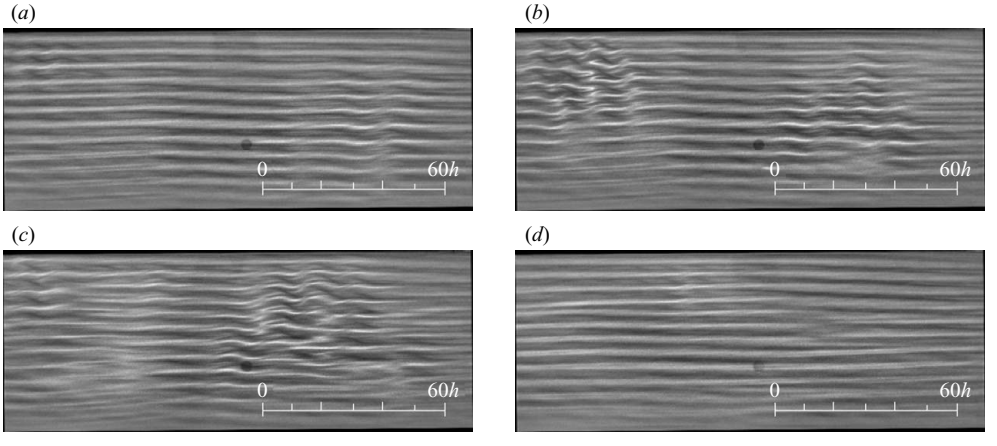

FIGURE 10. Spatio-temporally intermittent three-dimensional roll cells in a laminar flow with two-dimensional roll cell (COU3Ds). At $\Delta T = 0$ s, 12 s, 24 s and 50 s from (*a*) to (*d*). $Re = 151$, $\Omega = 1.32$.

two-dimensional→three-dimensional→two-dimensional→ $\cdots$. Therefore, in this paper, such case is termed COU3Ds. Nagata & Kawahara (2004) investigated the instability of the periodic (quaternary) solutions bifurcating from the three-dimensional (tertiary) solution and reported that the oscillatory instabilities gave rise to three-dimensional time-periodic motions, i.e. temporally intermittent three-dimensional roll cells, within a certain range of Ω. It was confirmed by their simulation that the periodic solutions at $Re = 100$ had been observed for $\Omega = 2.1$–8.0. Our observation with respect to COU3Ds is in agreement with this. In a higher Re region than COU3Ds, disordered turbulent-like motion occurs for a short period after the decay of three-dimensional roll cells. In figure 11, we have two other cases of intermittent development. Figure 11(a) shows a sequence of seven photographs following the development of a flow consisting mainly of three-dimensional roll cells; however, in this case the roll cells are unstable, break down and two two-dimensional cells appear in small regions, which after a while start to become three-dimensional again. This is a repeating, but random, process occurring across the full flow field.

Figure 11(b), on the other hand, is for a higher Reynolds number where both two-dimensional and three-dimensional cells appear in the flow field, but when the three-dimensional cells break down, the flow field seems to first become turbulent like. After a while, the turbulence decays and new two-dimensional and three-dimensional cells appears again. This is also a repeated process.

Finally, we show photographs (figure 12) where the basic flow field consists of unstable three-dimensional roll cells, which means that they break down to unorganized laminar-like motion (figure 12a) or a turbulence-like state, which we denote by quasi-turbulence (figure 12b). In this case, we are closer in parameter space to the region of the stable three-dimensional roll cells.

5.1.5. *Meandering laminar roll cells*

We have also found a region which we call stable meandering two-dimensional roll cells. This region borders to the three-dimensional roll-cell region, but it seems that the roll cells have a quite different internal structure in the three-dimensional case (figure 13). In the two-dimensional meandering case, the internal structure seems to change as compared to the straight two-dimensional cells, whereas the three-dimensional cells seem to have a complicated inner structure.

5.1.6. *Laminar two-dimensional roll cells at high rotation rates*

At high Ω and Re quite far away from the linear stability boundary, it is possible to again obtain two-dimensional roll cells. Figure 14 shows an example of such structures. The boundaries between the light and dark regions in the flow field are sharper than those for low Ω, and the dark regions seem to have some internal structure as well. This photograph is taken at the border of two-dimensional meandering roll cells, and as seen in figure 15 the flow field for these parameters changes slowly from meandering two-dimensional cells to straight ones. In the blow-up of the photographs in figure 15, the interior structure of the roll cells can be viewed in some more detail. If Ω is increased to become larger than Re, the two-dimensional roll cells must be suppressed because it approaches the stability boundary given by (2.8).

5.2. *Turbulent Couette flow*

In this section, we describe various regions in parameter space where the flow is fully turbulent but where rotation may give rise to roll-cell structures that seem to be overlaid on the turbulence. We chose mainly a Reynolds number of $Re = 751$ and then change Ω (i.e. Case-Re) to illustrate the different flow regimes.

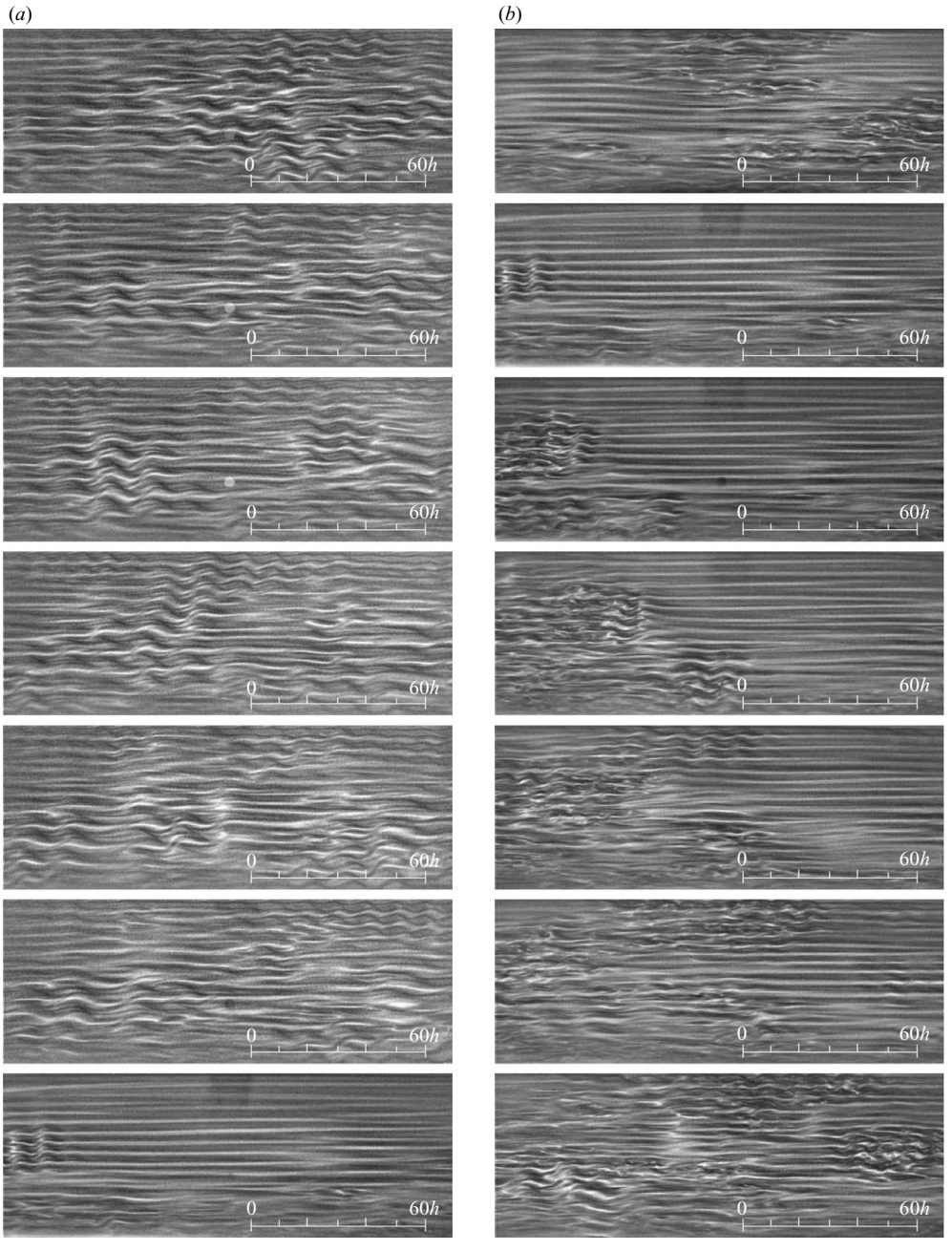

FIGURE 11. Spatio-temporally intermittent three-dimensional roll cells and their breakdown to turbulence (QTR3Ds). (*a*) $Re = 148$, $\Omega = 2.58$; (*b*) $Re = 300$, $\Omega = 1.04$. The time interval between photographs is 4 s (*a*) or 5 s (*b*).

5.2.1. *Turbulent Couette flow: featureless*

First, we describe briefly the fully turbulent case at high Reynolds numbers with weak positive rotation or moderate negative rotation. In figure 16(*a*), a short time (1/100 s) exposure is shown giving an instantaneous picture of the flow field exhibiting many

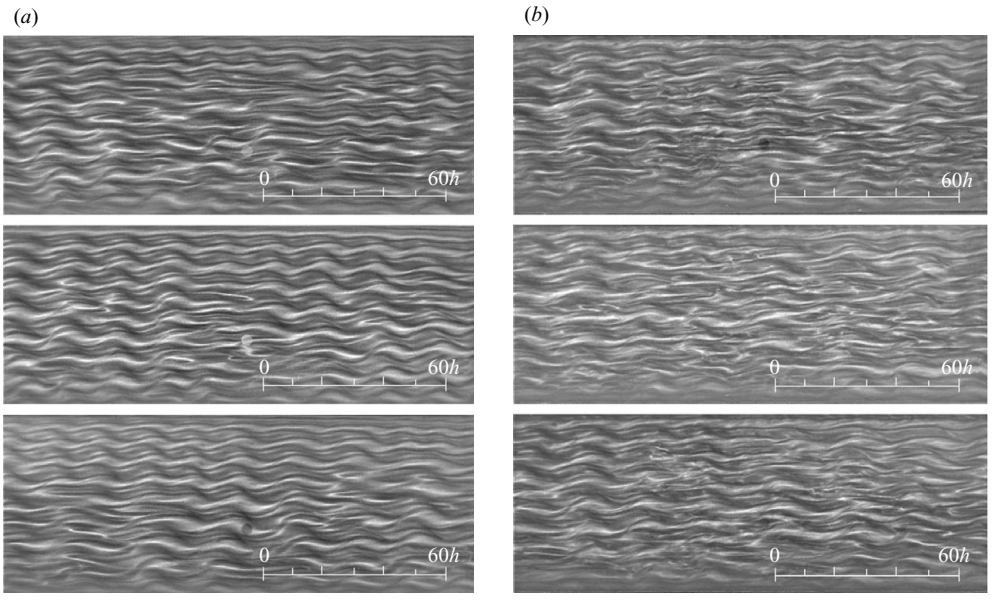

FIGURE 12. Unstable three-dimensional roll cells (QTR3D). (*a*) $Re = 151$, $\Omega = 8.36$; (*b*) $Re = 250$, $\Omega = 10.6$. The time interval between photographs is about 200 s (*a*) or 8 s (*b*).

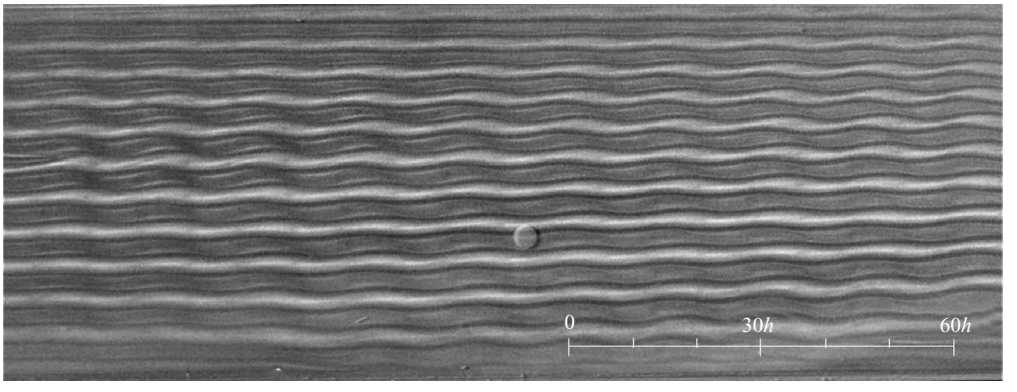

FIGURE 13. Stable meandering two-dimensional roll cells in laminar flow (COU2Dm); $Re = 147$, $\Omega = 20.1$.

small-scale turbulent structures. For $Re = 751$ and $\Omega = 1.08$, the turbulence turnover time scale is $\tau_o = 0.029$ s. This exposure time is, therefore, a reasonable compromise for a good still photograph.

In figure 16(*b*), we instead show a rather long-time exposure of the same flow field, which then averages out the small-scale structures and show elongated streamwise structures. Similar structures are also found in the case of $\Omega = 0$ and are neither induced nor affected by the rotation in this case. For the non-rotating turbulent case, it is well known that the central part contains large-scale streamwise velocity fluctuation extending over a very long streamwise distance, which is caused by large longitudinal vortical structures, as indicated by Lee & Kim (1991). There exists a mechanism, not clarified yet, in Couette flow that can sustain large-scale streamwise vortex structures (Kitoh, Nakabayashi & Nishimura 2005). Direct

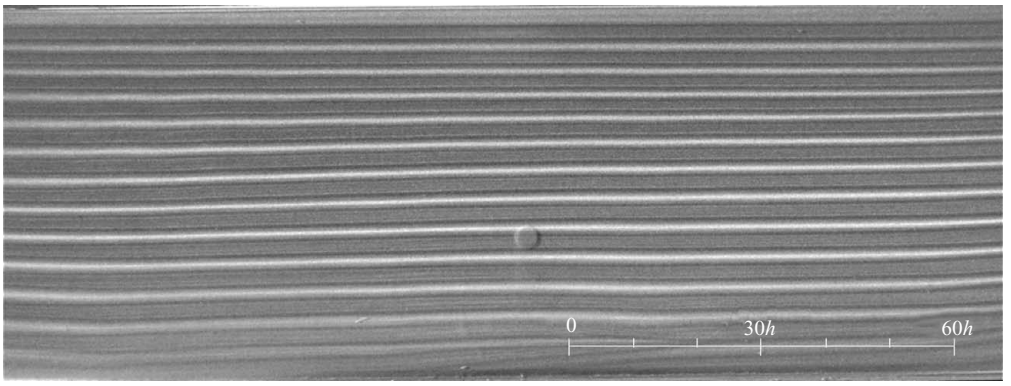

FIGURE 14. Stable two-dimensional roll cells in laminar flow (COU2Dh) at high Rotation number; $Re = 178$, $\Omega = 24.6$.

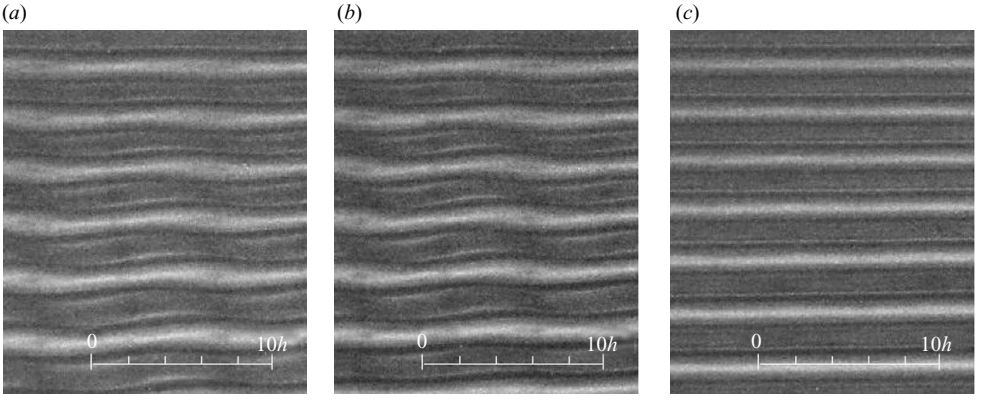

FIGURE 15. Sequential changes of structures from meandering two-dimensional roll cells to straight roll cells of the flow field at every 180 s (*a–c*). $Re = 178$, $\Omega = 24.6$.

numerical simulations with a sufficiently long computational domain were performed by Komminaho *et al.* (1996) and Tsukahara, Kawamura & Shingai (2006), and they revealed that the vortical structures are of finite size and stationary neither in time nor in space but fluctuating around their average position. According to their result, the streamwise length and the spanwise separation of the vortical structure are about 5–6h and 2h for $Re = 750$, respectively. The finite elongated structures we observed in figure 16(*b*) are comparable in size to the vortical structure and specifically different from a roll cell caused by the Coriolis force. This flow, labelled TUR, lacks any apparent roll cell except the vortical structures and is thus termed as 'featureless turbulence'.

Figure 16(*c*) is also a long-time exposure for a case $Re = 948$ with large negative rotation, $\Omega = -14.9$. The short-time exposure is similar to that in figure 16(*a*); however, as can be seen, the elongated structures have more or less disappeared in figure 16(*c*). Tsukahara *et al.* (2006) showed that the large-scale vortical structure became more prominent and elongated as Re increased from 750 to 2150. However, the flow under the negative rotation indicates no large-scale structure as well as roll

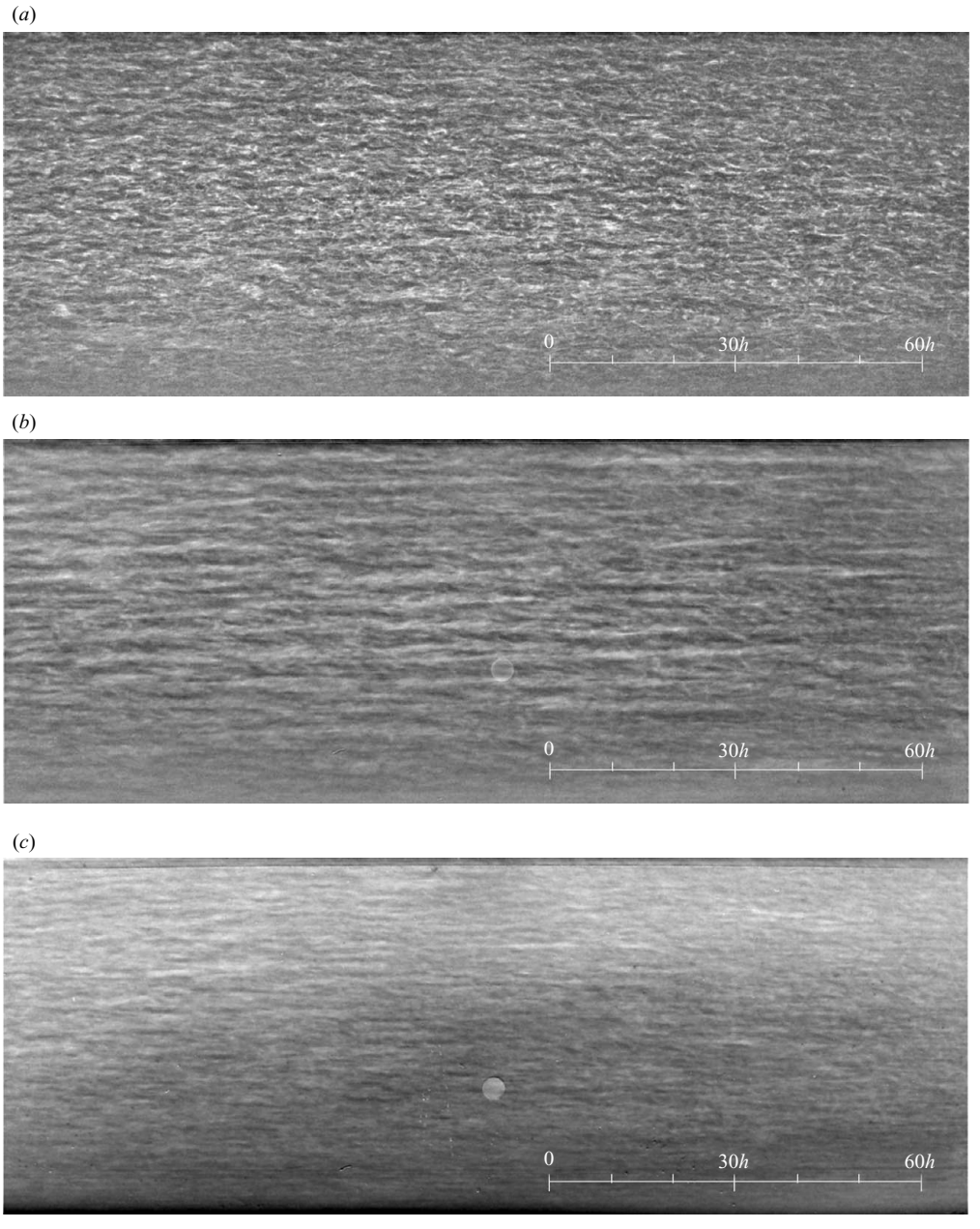

FIGURE 16. Featureless turbulent flow (TUR); (*a*,*b*) $Re = 751$, $\Omega = 1.08$; (*c*) $Re = 948$, $\Omega = -14.9$. The exposure time is 1/100 s in (*a*), 2.0 s in (*b*,*c*).

cells. The dominant visible length scale was smaller than the channel width. This is probably an effect of the stabilizing rotation.

5.2.2. *Turbulent Couette flow: with stable two-dimensional roll cells*

Increasing the rotation rate (still with $Re = 751$), we go into a region where roll cells are formed and seem to overlay the turbulence without any direct interaction (figure 17). Figure 17(*a*) (short-time exposure) shows rather homogeneous fine-scale

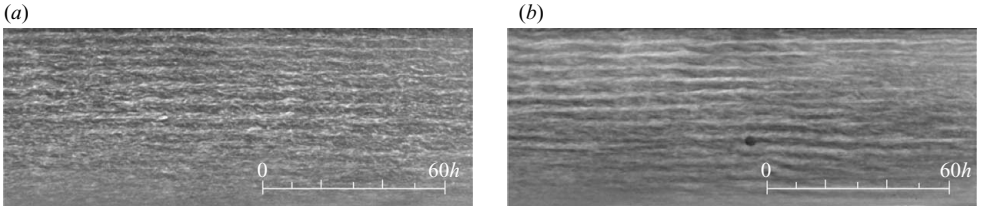

FIGURE 17. Stable two-dimensional roll cells in turbulent flow (TUR2D); $Re = 751$, $\Omega = 5.03$. The exposure time is 1/80 s in (*a*) and 2.0 s in (*b*).

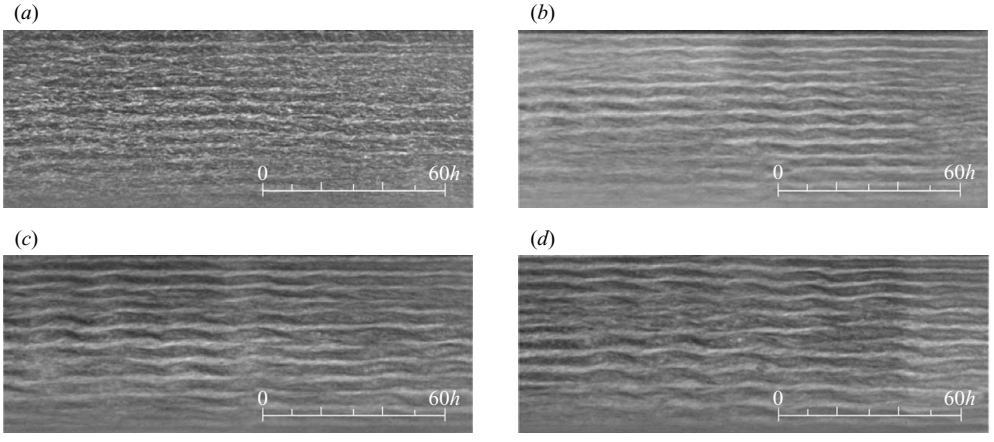

FIGURE 18. Spatio-temporally intermittent three-dimensional roll cells in a turbulent flow (TUR3Ds) at $Re = 751$; (*a*,*b*) $\Omega = 8.78$, (*c*) $\Omega = 14.4$, (*d*) $\Omega = 16.2$. The exposure time is 1/80 s in (*a*) and 2.0 s in (*b–d*).

turbulent structures, while the time-averaged (a long exposure time) flow field reveals the coexistence of two-dimensional roll cells (figure 17*b*) of a much larger scale. When compared to the time-averaged field for zero or weak rotation shown in figure 16(*b*), the dominant structures show a regular pattern in the spanwise direction and are elongated in the streamwise direction. These features are common to the two-dimensional roll cells in the laminar background (cf. figure 7).

5.2.3. *Turbulent Couette flow: with spatio-temporal developing three-dimensional roll cells*

In figure 18, we see an example where the flow field is turbulent on top of the roll cells. However, with the long time averaging, it is clear that the roll cells are not stable but that there exist regions where the roll cells have disappeared and other regions where they still are strong. These regions are not stationary, and we denote the flow as spatio-temporally developing.

5.2.4. *Turbulent Couette flow: with stable three-dimensional roll cells*

The stationary laminar three-dimensional roll cells have their counterpart also for high Reynolds numbers where the flow is turbulent. Figure 19 shows both a short and long time exposure of the flow field. The long-time exposure is quite similar to the laminar case in its structure; however, there is a distinct difference in both the spanwise and streamwise scales.

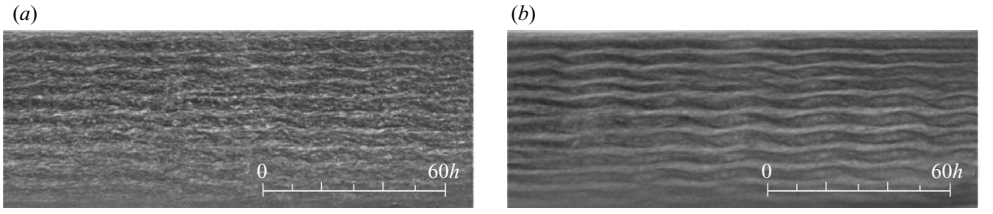

FIGURE 19. Stable three-dimensional roll cells in a turbulent flow (TUR3D); $Re = 751$, $\Omega = 21.8$. The exposure time is 1/80 s in (a) and 2.0 s in (b).

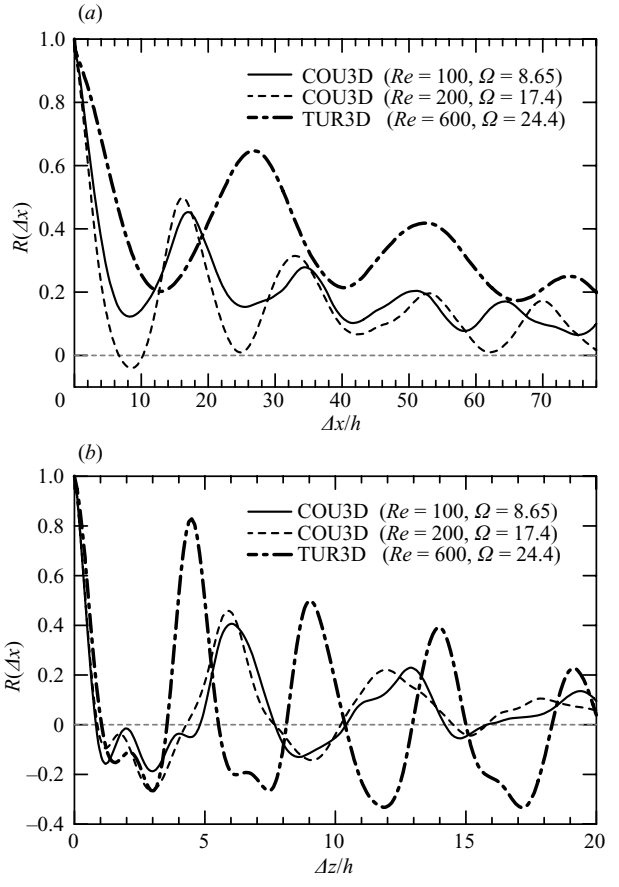

FIGURE 20. Two-point correlation coefficient of light intensity, for the flows with stable three-dimensional roll cells, as a function of streamwise distance Δx or spanwise distance Δz. The cases of COU3D correspond to those shown in figure 9, whereas the case of TUR3D is at slightly lower Reynolds number than that for the photograph given in figure 19(b).

Figure 20 shows both the streamwise and spanwise correlations of the three-dimensional stable structures in the laminar and turbulent cases. In the turbulent case, the correlation is obtained from a long-time exposure of the flow such as in figure 19(b). The laminar ones (at two different combinations of Re and Ω) give a streamwise length scale of about $16h$, whereas in the turbulent case the scale is about $26h$. For the spanwise correlation, on the other hand, the turbulent case gives the shortest spanwise length scale of about $4.5h$, whereas in the laminar cases the

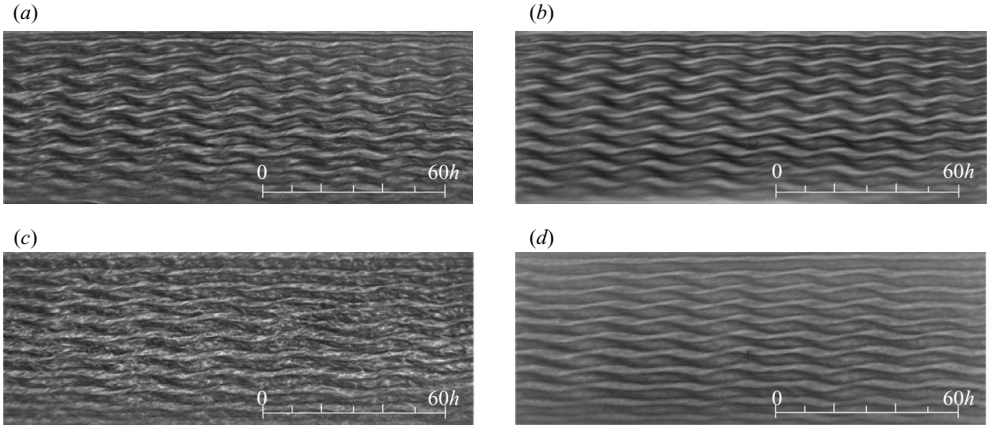

FIGURE 21. Contained turbulence in three-dimensional roll cells (CNT3D); the exposure time is 1/30 s in (*a*), 1/100 s in (*c*), 2.0 s in (*b,d*). (*a,b*) $Re = 300$, $\Omega = 21.1$; (*c, d*) $Re = 500$, $\Omega = 25.8$.

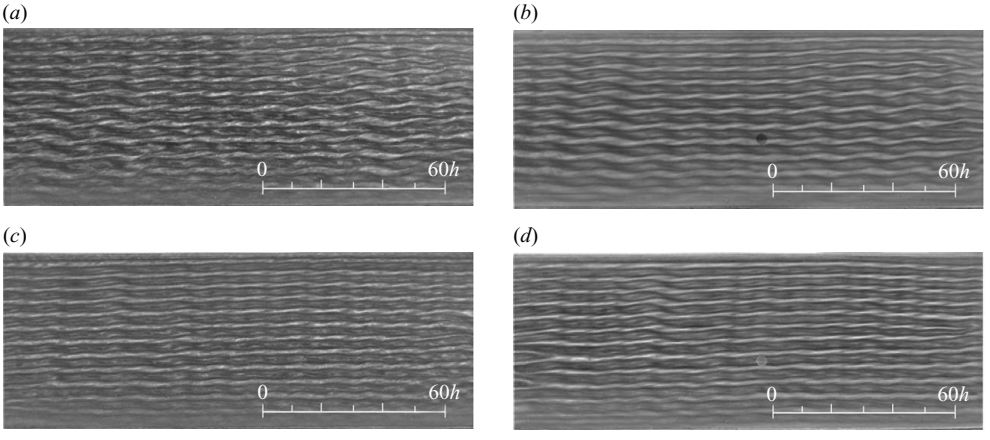

FIGURE 22. Contained turbulence in two-dimensional meandering roll cells (CNT2Dm); the exposure time is 1/30 s in (*a,c*), 2.0 s in (*b,d*). (*a,b*) $Re = 350$, $\Omega = 25.5$; (*c,d*) $Re = 350$, $\Omega = 29.0$.

major correlation peak is at $6h$. In comparison to the correlation function for the purely two-dimensional laminar case (figure 8), these correlation functions gave some local peaks, which signifies that the flow structures have a more complicated structure here.

5.3. *Contained turbulence in roll cells*

In another region of parameter space at high Re and Ω, we find that the turbulence seems to be contained in the roll cells and not connected to turbulence in neighbouring cells. This observation has been done both for three-dimensional roll cells (figure 21) and for two-dimensional meandering cells (figure 22). Considering the scenario of roll cells modifications in the laminar background described in § 5.1, it is conjectured that the two-dimensional meandering cells that are embedded in turbulence should change to straight cells, labelled 2Dh, at high rotation numbers.

If the rotation number is increased further, the turbulent motion and the roll cells are expected to be quenched for $\Omega > Re$, as demonstrated by Alfredsson & Tillmark (2005).

5.4. *Intermittent turbulence, turbulent stripes or turbulent spots*

For stabilizing rotation, there is a wedge-shaped region in the flow regime diagram (figure 2) where the flow is found to have coexisting laminar and turbulent regions. To describe the development in this region, let us decrease the Reynolds number at a fixed (negative) Ω. For high enough Reynolds number the flow is fully turbulent (which we call featureless turbulence). Decreasing Re, we enter a region that we denote the intermittent turbulence region (INT), that is a sub-region of the above-mentioned wedge-shaped region. Most part of the flow field shows featureless turbulence, although in some randomly spaced and shaped regions, a localized laminar region appears for a short time. A typical such flow case is seen in figure 23(a). By further decreasing Re, we enter a region (TRS) where stripes are observed which stretch across the channel and consist of a periodic alternation of turbulent and laminar bands. The inclination of the stripes seems to decrease with decreasing Reynolds number. Such a flow situation is seen in figure 23(b). However, the orientation of the inclination is not given by the apparatus but changes from case to case. The pattern itself is essentially stationary in space and persists for many hours, it presumably has an indefinite lifetime. Decreasing Re even further there is another, relatively narrow, sub-region (SPT) neighbouring the laminar Couette flow region where isolated turbulent spots move around randomly, they are born and they die (see figure 23c). Note that with increasing negative rotation, the Reynolds number for which the flow is fully laminar increases showing the stabilizing effect of rotation.

Similarly, earlier PCF experiments produced localized turbulent patches as the result of a distinct transition to a fairly regular pattern with finite wavelengths of the order of 40–60h (cf. Prigent *et al.* 2002; Prigent & Dauchot 2005). Here, the wavevector is in a direction perpendicular to the relevant observed turbulence bands. The wavelength of the pattern in figure 23(b) is approximately 60h, and the wavevector is inclined at an angle of about 37° against the streamwise direction. Although only a few turbulent stripes are observed simultaneously because of the rather low aspect ratio of the present channel, the wavelength and the inclination angle roughly agree with those obtained by Prigent *et al.* (2002), and it is hypothesized that the turbulent stripes in the RPCF (as well as PCF) and the spiral turbulence in TCF are similar.

Figure 24 shows how this pattern changes when the Reynolds number decreases for a given Ω. For the lowest Reynolds number, the flow is close to the SPT region. However, the range of Reynolds numbers where one can observe isolated turbulent spots is quite narrow even if the stabilizing rotation rate $|\Omega|$ is high. On the other hand, as Re increases the width of the turbulent band increases until no well-defined large-scale pattern can be observed in the INT region.

6. Summary and conclusions

We have reported the first extensive mapping of the Re–Ω plane in a rotating plane Couette flow. Our measurements are taken in the ranges $0 < Re < 1050$ and $-27 < \Omega < 30$, thereby coveringlaminar, transitional and turbulent flow regimes. During this mapping, we have identified 17 different flow states, both laminar and turbulent, with and without roll cells, as well as states that can be described as transitional, i.e. states that contain both laminar and turbulent regions at the same

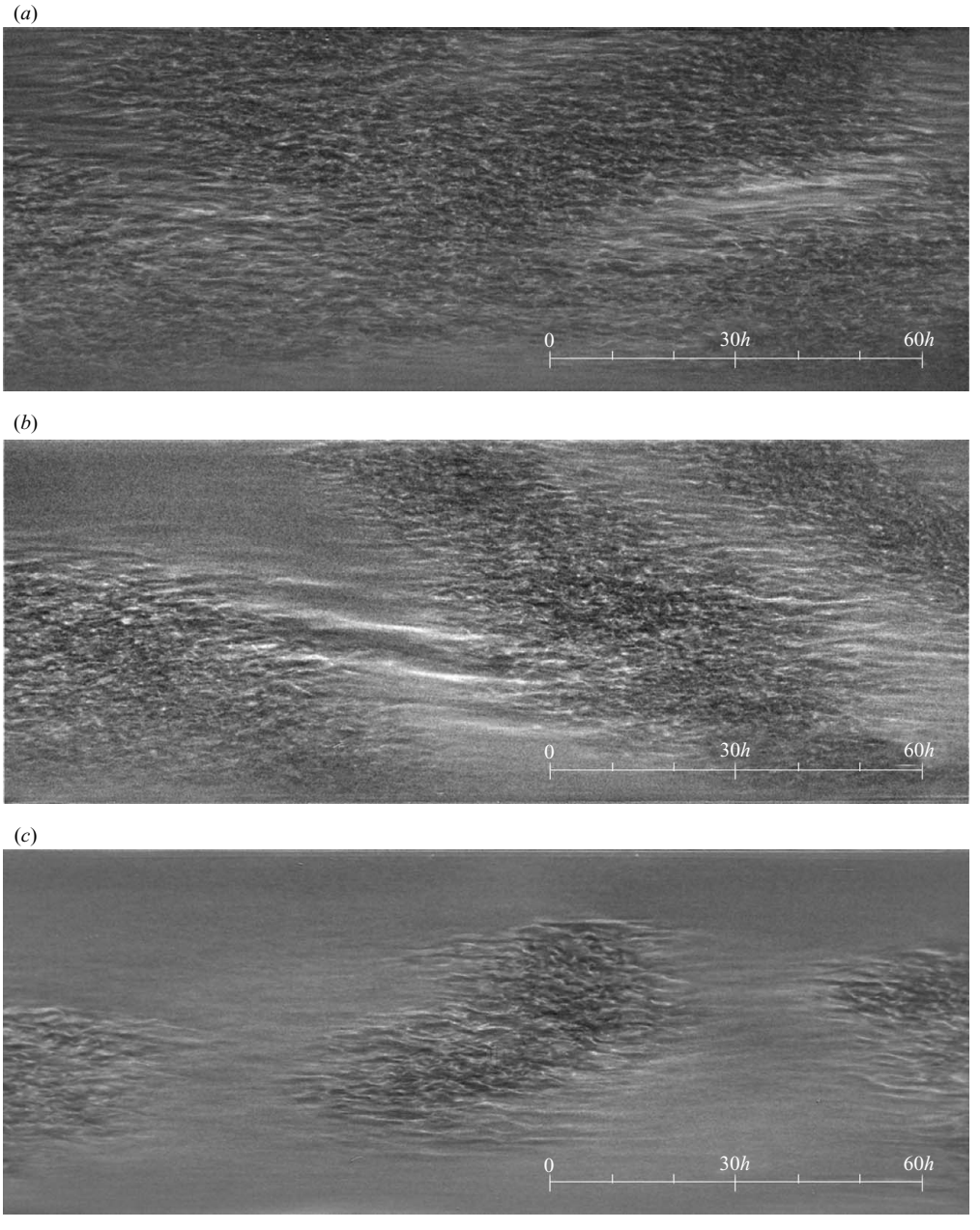

FIGURE 23. Intermittent turbulence: (*a*) localized laminar region occurs in turbulent flow (INT) at $Re = 751$, $\Omega = -14.4$; (*b*) turbulent stripes (TRS) for $Re = 751$, $\Omega = -25.8$; (*c*) turbulent spots in a laminar flow (SPT) at $Re = 600$, $\Omega = -24.4$.

time. The Re–Ω plane has been covered by keeping Ω constant varying Re and vice versa.

The mapping has been documented not only through flow visualization using reflective flakes and still photography but also through direct observation by the naked eye. In order to enhance the contrast of the photographs, they have been digitally enhanced to take into account the varying brightness of the pictures. For

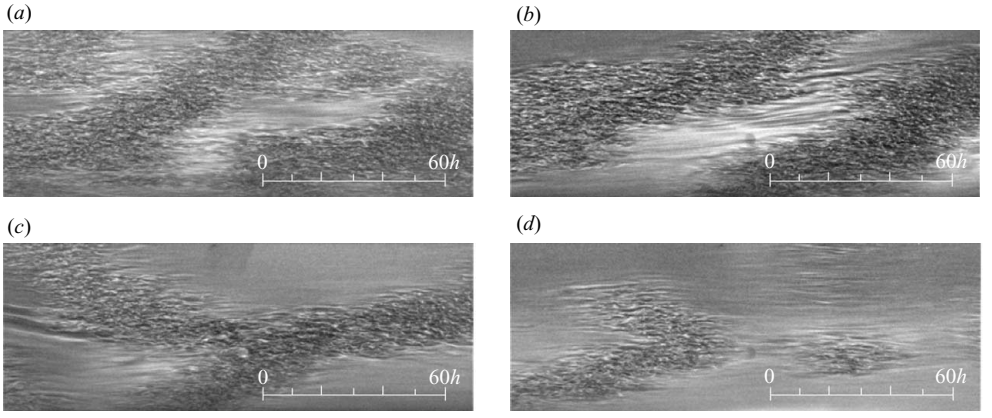

FIGURE 24. Sequence change of turbulent stripes as Re was decreased for fixed $\Omega = -14.9$: Re is 720, 654, 591 and 563 in (a–d).

some flow fields, photographs have been taken with both short- and long-time exposures, the short-time exposure gives an instantaneous picture of the turbulent flow field, whereas the long-time exposure averages the small, rapidly varying scales and only shows the large scales.

In some cases the photographs have been used to obtain the scales of the structures by applying correlation techniques to the light intensity of the photographs. In this way, it was easy to obtain, in an objective manner, both the spanwise and streamwise wavelengths of the flow structures.

The conclusions from our study can be summarized as follows:

(i) The Re–Ω plane of rotating plane Couette flow shows a very rich atlas of various flow states, comparable with that found for Taylor–Couette flow. Some of the flow states seem to have similar characteristics whereas others seem to be unique for the present case.

(ii) The RPCF does not seem to be susceptible to hysteresis effects, i.e. it is not sensitive to from which direction a certain point in the Re–Ω plane is reached.

(iii) The transitional Reynolds number obtained without rotation is consistent with the values obtained earlier in the present apparatus. This value is about 10 % higher than the value obtained by other groups and the reason for this is still not clear.

(iv) For stabilizing rotation, not only the transitional Reynolds number increases as expected but also the range of Reynolds numbers where a striped pattern of inter-weaved laminar–turbulent regions is observed becomes wider, and the width increases with increasing stabilizing Ω. In the present flow, only a few (2–3) turbulent stripes could be observed simultaneously because of the rather low aspect ratio of the present channel. The range of Reynolds numbers where one can observe isolated turbulent spots is however quite narrow, independent of the stabilizing rotation rate.

(v) For destabilizing rotation, a number of interesting phenomena are observed. The laminar regime regions, where stable three-dimensional roll cells are observed, seem to be consistent with the results of Nagata (1998) and Hiwatashi *et al.* (2007). For other parameter values, the three-dimensional roll cells are spatially and temporally intermittent, i.e. they are suddenly observed on top of two-dimensional cells as predicted by Nagata & Kawahara (2004), whereafter they decay. In other ranges, three-dimensional cells break down to turbulence and then they are again re-established in a repeating pattern.

(vi) At high Re and/or high Ω, roll cells are observed to become turbulent, although in the photographs the underlying roll-cell structure is still observed. Both two-dimensional and three-dimensional turbulent roll cells have been observed. By taking long-time exposures of the flow, it has been shown that the roll-cell structures are sustained more or less as in the laminar case, although both the spanwise and the streamwise (in the three-dimensional case) wavelengths increase.

The observations put forward in this paper give many opportunities to study the effect of rotation on the stability, transition and turbulence in shear flows. With the mapping carried out, it is easy to find the parameter range where a specific flow state occurs. This will be especially valuable for those studying such flows and phenomena in detail using direct numerical simulations because the mapping gives a good indication where different states can be found.

This work has been carried out within the Linné Flow Centre, which is supported by the Swedish Research Council. The first author (T.T.) was supported by Japan Society for the Promotion of Science (JSPS) Fellowship (18-81) and also by Research Center for the Holistic Computational Science. Part of this paper was written when the third author (P.H.A.) was invited to Tokyo University of Science. Professor Hiroshi Kawamura is thankfully acknowledged for taking the initiative to this cooperation between KTH and TUS.

REFERENCES

Alfredsson, P. H. & Persson, H. 1989 Instabilities in channel flow with system rotation. *J. Fluid Mech.* **202**, 543–557.

Alfredsson, P. H. & Tillmark, N. 2005 Instability, transition and turbulence in plane Couette flow with system rotation. In *IUTAM Symposium on Laminar Turbulent Transition and Finite Amplitude Solutions* (ed. T. Mullin & R. R. Kerswell), *Fluid Mechanics and Its Applications*, vol. 77, pp. 173–193. Springer.

Andereck, C. D., Liu, S. S. & Swinney, H. L. 1986 Flow regimes in a circular Couette system with independently rotating cylinders. *J. Fluid Mech.* **164**, 155–183.

Barkley, D. & Tuckerman, L. S. 2005 Computational study of turbulent laminar patterns in Couette flow. *Phys. Rev. Lett.* **94**, 014502.

Barkley, D. & Tuckerman, L. S. 2007 Mean flow of turbulent–laminar patterns in plane Couette flow. *J. Fluid Mech.* **576**, 109–137.

Barth, W. L. & Burns, C. A. 2007 Virtual rheoscopic fluids for flow visualization. *IEEE Trans. Visual. Comp. Graphics* **13**, 1751–1758.

Bech, K. H. & Andersson, H. I. 1996 Secondary flow in weakly rotating turbulent plane Couette flow. *J. Fluid Mech.* **317**, 195–214.

Bech, K. H. & Andersson, H. I. 1997 Turbulent plane Couette flow subject to strong system rotation. *J. Fluid Mech.* **347**, 289–314.

Bech, K. H., Tillmark, N., Alfredsson, P. H. & Andersson, H. I. 1995 An investigation of turbulent plane Couette flow at low Reynolds numbers. *J. Fluid Mech.* **286**, 291–325.

Carey, C. S., Schlender, A. B. & Andereck, C. D. 2007 Localized intermittent short-wavelength bursts in the high-radius ratio limit of the Taylor–Couette system. *Phys. Rev.* E **75**, 016303.

Chandrasekhar, S. 1961 *Hydrodynamic and Hydromagnetic Stability*. Oxford University Press.

Coles, D. 1965 Transition in circular Couette flow. *J. Fluid Mech.* **21**, 385–425.

Dauchot, O. & Daviaud, F. 1995 Finite amplitude perturbation and spots growth mechanism in plane Couette flow. *Phys. Fluids* **7**, 335–343.

Daviaud, F., Hegseth, J. & Bergé, P. 1992 Subcritical transition to turbulence in plane Couette flow. *Phys. Rev. Lett.* **69**, 2511–2514.

Drazin, P. G. & Reid, W. H. 1981 *Hydrodynamic Stability*. Cambridge University Press.

Faisst, H. & Eckhardt, B. 2000 Transition from the Couette–Taylor system to the plane Couette system. *Phys. Rev.* E **61**, 7227–7230.

Hegseth, J. J., Anderech, C. D., Hayot, F. & Pomeau, Y. 1989 Spiral turbulence and phase dynamics. *Phys. Rev. Lett.* **62**, 257–260.

Hiwatashi, K., Alfredsson, P. H., Tillmark, N. & Nagata, M. 2007 Experimental observations of instabilities in rotating plane Couette flow. *Phys. Fluids* **19**, 048103.

Johnston, J. P., Halleent, R. M. & Lezius, D. K. 1972 Effects of spanwise rotation on the structure of two-dimensional fully developed turbulent channel flow. *J. Fluid Mech.* **56**, 533–557.

Kitoh, O., Nakabayashi, K. & Nishimura, F. 2005 Experimental study on mean velocity and turbulence characteristics of plane Couette flow: low-Reynolds-number effects and large longitudinal vortical structure. *J. Fluid Mech.* **539**, 199–227.

Komminaho, J., Lundblad, A. & Johansson, A. V. 1996 Very large structures in plane turbulent Couette flow. *J. Fluid Mech.* **320**, 259–285.

Koschmieder, E. L. 1993 *Bénard Cells and Taylor Vortices*. Cambridge University Press.

Lee, M. J. & Kim, J. 1991 The structure of turbulence in a simulated plane Couette flow. In *Proceedings of Eighth Symposium on Turbulent Shear Flows* (ed. F. Durst *et al.*), Munich, Germany, paper 5-3, 6 pp.

Lezius, D. K. & Johnston, J. P. 1976 Roll-cell instabilities in rotating laminar and turbulent channel flows. *J. Fluid Mech.* **77**, 153–175.

Lundbladh, A. & Johansson, A. V. 1991 Direct simulation of turbulent spots in plane Couette flow. *J. Fluid Mech.* **229**, 499–516.

Nagata, M. 1998 Tertiary solutions and their stability in rotating plane Couette flow. *J. Fluid Mech.* **358**, 357–378.

Nagata, M. & Kawahara, G. 2004 Three-dimensional periodic solutions in rotating/non-rotating plane Couette flow. In *Advances in Turbulence X, Proceedings of the Tenth European Turbulence Conference* (ed. H. I. Andersson & P. Å. Krogstad), pp. 391–394. CIMNE.

Prigent, A. & Dauchot, O. 2005 Transitional to versus from turbulence in subcritical Couette flows. In *IUTAM Symposium on Laminar Turbulent Transition and Finite Amplitude Solutions* (ed. T. Mullin & R. R. Kerswell), *Fluid Mechanics and Its Applications*, vol. 77, pp. 195–219. Springer.

Prigent, A., Grégoire, G., Chaté, H., Dauchot, O. & van Saarloos, W. 2002 Large-scale finite-wavelength modulation within turbulent shear flows. *Phys. Rev. Lett.* **89**, 014501.

Rayleigh, L. 1880 On the stability, or instability, of certain fluid motions. *Proc. Lond. Math. Soc.* **174**, 57–70.

Reynolds, O. 1883 An experimental investigation of the circumstances which determine whether the motion of water shall be direct or sinuous, and of the law of resistance in parallel channels. *Phil. Trans. R. Soc. Lond.* A **174**, 935–982.

Savaş, Ö. 1985 On flow visualization using reflective flakes. *J. Fluid Mech.* **152**, 235–248.

Schmid, P. J. & Henningson, D. S. 2001 *Stability and Transition in Shear Flows*, Applied Mathematical Sciences, vol. 142. Springer.

Taylor, G. I. 1923 Stability of a viscous liquid contained between two rotating cylinders. *Phil. Trans. R. Soc. Lond.* **223**, 289–343.

Tillmark, N. & Alfredsson, P. H. 1990 An experimental study of transition in plane Couette flow. In *Advances in Turbulence III, Proceedings of the Third European Turbulence Conference* (ed. A. V. Johansson & P. H. Alfredsson), pp. 235–242. Springer.

Tillmark, N. & Alfredsson, P. H. 1992 Experiments on transition in plane Couette flow. *J. Fluid Mech.* **235**, 89–102.

Tillmark, N. & Alfredsson, P. H. 1996 Experiments on rotating plane Couette flow. In *Advances in Turbulence VI, Proceedings of the Sixth European Turbulence Conference* (ed. S. Gavrilakis, L. Machiels & P. A. Monkewitz), pp. 391–394. Kluwer Academic.

Tsukahara, T., Kawamura, H. & Shingai, K. 2006 DNS of turbulent Couette flow with emphasis on the large-scale structure in the core region. *J. Turbul.* **7** (19), 16 pp.

Tsukahara, T., Seki, Y., Kawamura, H. & Tochio, D. 2005 DNS of turbulent channel flow at very low Reynolds numbers. In *Proceedings of Fourth International Symposium on Turbulence and Shear Flow Phenomena* (ed. J. A. C. Humphrey *et al.*), pp. 935–940.